ELSEVIER

Journal of Structural Geology 29 (2007) 1301–1314

JOURNAL OF STRUCTURAL GEOLOGY

www.elsevier.com/locate/jsg

Reaction weakening and emplacement of crystalline thrusts: Diffusion control on reaction rate and strain rate

Kieran O'Hara

Department of Earth and Environmental Sciences, University of Kentucky, Lexington, KY 40506, USA

Received 1 October 2006; received in revised form 22 April 2007; accepted 23 April 2007
Available online 5 May 2007

Abstract

In the southern Appalachians, the Blue Ridge–Piedmont crystalline thrust sheet was emplaced onto low-grade Late Precambrian and Paleozoic sedimentary rocks in the footwall along a basal detachment consisting of phyllosilicate-rich mylonites (phyllonites). The phyllonites developed first by mechanical breakdown of feldspar followed by chemical breakdown to white mica in the presence of a pore fluid. Diffusion of solute in the pore fluid is the rate limiting step in controlling reaction rate and also the strain rate. Assuming solute diffusion follows the Stokes–Einstein equation, the shear strain rate is given by $d\gamma/dt = 2^n\omega kT/5\eta r x^2$ for shear stress $\geq$20 MPa, where n is a constant, ω is a geometric factor, k is Boltzmann's constant, T is absolute temperature, η is water viscosity, r is the atomic radius of the diffusing species, and x is the diffusion distance. A bulk diffusion coefficient in the range of $\sim 10^{-10}$ to 10^{-12} m^2/s over distances of 10–100 m results in strain rates of 10^{-14} to 10^{-13} s^{-1} in the temperature range 200–400 °C. It is concluded that greenschist grade crystalline thrust sheets develop on pre-existing basement faults that become weak during reaction softening and localize into high strain phyllonite zones in which pore fluid diffusion controls reaction rate and strain rate.

Keywords: Strain softening; Phyllonite; Pore fluid diffusion; Southern Appalachians

1. Introduction

A common feature of the internal portions of many mountain belts is the presence of crystalline thrust sheets that have traveled far from their source (Armstrong and Dick, 1974; Boyer and Elliott, 1982; Laubscher, 1983; Hatcher and Hooper, 1992; Wibberley, 2005). The mechanism of emplacement of crystalline thrust sheets reflects the behavior of the continental crust during collisional processes, and is therefore important to understanding continental deformation. An influential model of continental crustal strength indicates a strong brittle upper crust that gives way to a weaker ductile lower crustal layer (Brace and Kohlstedt, 1980). In this model, the strength of faults in the upper crust increases with depth according to laboratory friction experiments (Byerlee, 1978), but at greater depths, temperature dominates over confining pressure and thermally activated mechanisms (such as dislocation creep in quartz and feldspar) control crustal strength below the brittle–ductile transition (Carter and Tsenn, 1987). For example, crystalline thrust sheet emplacement is commonly explained by weakness at the base of the brittle crust, whereby thrust slices become detached at a depth corresponding to the brittle–ductile transition (Armstrong and Dick, 1974; Boyer and Elliott, 1982; Hatcher and Hooper, 1992). Several workers (Janecke and Evans, 1988; Wintsch et al., 1995; Imber et al., 2001; Wibberley, 2005), however, have pointed out that this model of the crust requires substantial modification in light of the widespread recognition that crustal faults are commonly phyllosilicate-rich mylonitic rocks (phyllonites). In this case, Byerlee-type friction or power law creep of quartz is unlikely to control strength in either the brittle or ductile regimes.

In the Blue Ridge province of the southern Appalachians the base of crystalline thrust sheets are commonly lined with phyllonites (Bryant, 1966; O'Hara, 1988; Newman and Mitra, 1993; Bailey, 1995). Understanding the behavior and strength

E-mail address: geokoh@uky.edu

0191-8141/$ - see front matter © 2007 Elsevier Ltd. All rights reserved.
doi:10.1016/j.jsg.2007.04.004

of these rock types is therefore important to understand the assembly of the internal portions of mountain belts. In this paper I propose a model for the rheology of phyllonites in which diffusion of solutes in a pore fluid controls reaction rate and strain rate. The model is applied to the emplacement of the Blue Ridge–Piedmont thrust in the southern Appalachians, but it is also applicable to crystalline thrusts in other orogenic belts emplaced under greenschist conditions.

2. Tectonic setting

Hatcher and Hooper (1992) distinguished several types of crystalline basement thrusts. Their type C thrusts (composite basement) are thin, stiff sheets that show little or no internal deformation and are inferred to have been emplaced as rigid blocks, typically under greenschist conditions. Examples include the Blue Ridge–Piedmont sheet which, on the basis of seismic reflection profiles (Cook et al., 1979), is one of the largest (>300 km wide). The Silvretta thrust sheet in the eastern Alps (Laubscher, 1983) and the Pelvoux Massif in the western Alps (Wibberley, 2005) are other examples. In the case of type C thrusts, it is commonly assumed that they become detached at a level in the crust corresponding to the "brittle–ductile" transition, which may correspond to the onset of crystal plasticity in quartz (e.g. Armstrong and Dick, 1974; Boyer and Elliott, 1982; Laubscher, 1983; Hooper and Hatcher, 1992).

Greenschist grade phyllonites are common along thrusts in the western Blue Ridge province of the southern Appalachians (Fig. 1; O'Hara, 1988, 1990; Bailey, 1995). In the more internal parts of the thrust sheet, the Grandfather Mountain window exposes similar rock types on the Linville Falls thrust (LFT, Fig. 1; Newman and Mitra, 1993), consistent with the idea that the entire sheet is underlain by similar mica-rich mylonites. Phyllonites along the Linville Falls thrust (LFT, Fig. 1) yield a Rb–Sr whole rock isochron of ~300 Ma, indicating a Pennsylvanian age of thrust emplacement (Schedl et al., 1992). Mylonites along thrusts to the east in the Central Blue Ridge yield older ages ($^{40}Ar/^{39}Ar$ and Rb–Sr mineral ages) of ~325 Ma indicating that the composite thrust sheet was assembled earlier, and then emplaced in sequence, piggyback-style, during the Alleghanian orogeny (Goldberg and Dallmeyer, 1997).

Along the frontal Blue Ridge thrust (Fig. 1), detailed mylonite studies at Hot Springs (Rector Branch thrust, Fig. 1; O'Hara, 1988, 1990) show thick (~80 m) phyllonite developed at the contact between basement rocks and underlying Late Precambrian clastic meta-sedimentary rocks. At Fries (Fig. 1), a wide (~1 km) zone of phyllonite is developed between Precambrian basement in the hanging wall and lower Paleozoic sediments and Precambrian basement in the footwall (O'Hara, 1990). At the Linville Falls thrust, phyllonites of 1–100 m thick are developed between granitic basement rocks in the hanging wall and Paleozoic quartzites in the footwall (Newman and Mitra, 1993). Farther to the north along strike in Virginia, mica-rich mylonites are also present within a wide (1–3 km) high strain zone (Rockfish Valley fault)

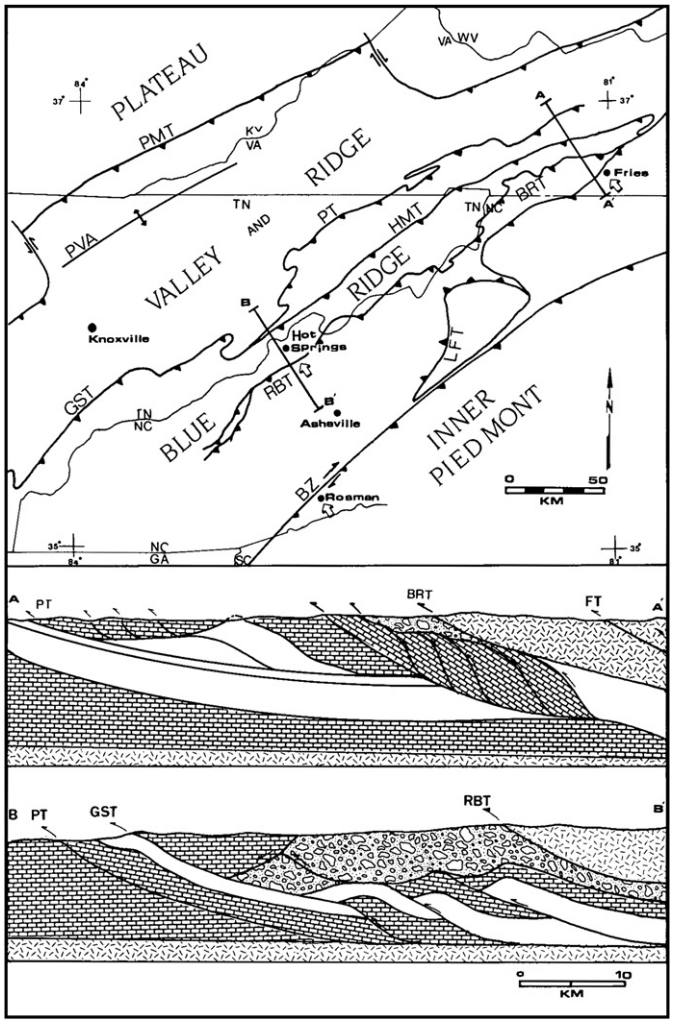

Fig. 1. Generalized geologic map of the southern Appalachians showing tectonic provinces and the tectonic boundaries between them. PMT, Pine Mountain thrust; PVA, Powell Valley anticline; PT, Pulaski thrust; BRT, Blue Ridge thrust; RBT, Rector Branch thrust; LFT, Linville Falls thrust; BZ, Brevard zone; FT, Fries thrust. Teeth on the upper plate of thrusts. Cross section A–A′ after Woodward and Gray (1985) and section B–B′ after Rast and Kohles (1985). Random stipple: Blue Ridge basement; conglomerate pattern: Late Precambrian clastic rocks (Snowbird Group); brick pattern: Paleozoic stratigraphic section.

within the Grenville basement (Bailey, 1995). Together, the Rector Branch–Fries–Rockfish Valley faults make up a major tectonic boundary in the western Blue Ridge province that can be traced along strike for 400 km in North Carolina and Virginia.

3. Deformation of feldspar and quartz in phyllonites

At Hot Springs, North Carolina (Fig. 1), the protolith rocks are coarse grained biotite gneisses with a weak foliation defined by aligned feldspars and biotite (Fig. 2a). Close to the Rector Branch thrust, these rocks become more strongly foliated with a weak to absent lineation, and biotite is retrograded to chlorite (Fig. 2b). Feldspars commonly show offset on brittle shears. Within fault zones, the rocks take on a schistose character with decreasing modal abundance of feldspar

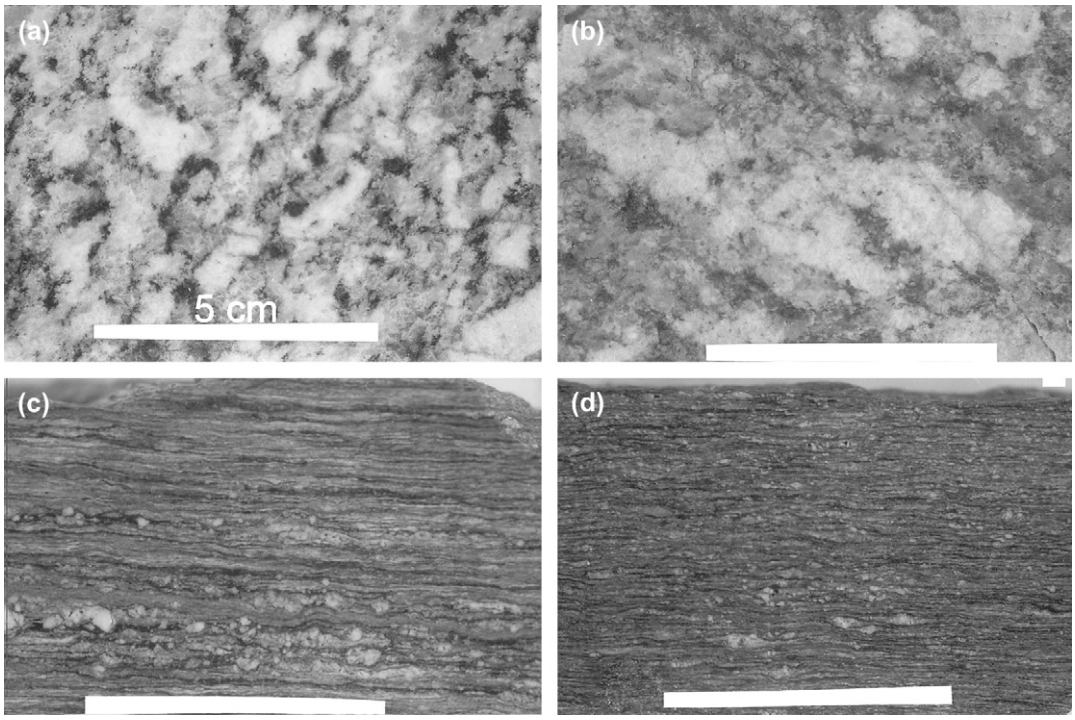

Fig. 2. Progressive mylonitization of basement gneiss (Max Patch granite). Scale bar 5 cm. (a) Typical biotite gneiss showing regional foliation. (b) Foliated gneiss with biotite retrograded to chlorite. Feldspars show brittle shears. (c) Phyllonite developed from granite gneiss showing relict rounded feldspar clasts in a matrix of white mica and chlorite that defines the mylonitic foliation. (d) Phyllonite in which most of the feldspar has been dissolved. The foliation shows conspicuous concentrations of insoluble accessory minerals such as apatite, zircon, epidote, tourmaline and iron oxides.

and increased abundance of fine-grained white mica (usually phengite) and chlorite (Fig. 2c). In more intensely deformed mylonites, the abundance of feldspar is low and the rocks are termed ultramylonites or phyllonites (Fig. 2d).

Microstructural observations in these rocks indicate that the feldspars deform in a brittle mode, fracturing mainly along their cleavage planes (Fig. 3). Alkali feldspars have two perfect cleavages on [001] and [010] and plagioclase has one perfect cleavage on [001] (Deer et al., 1992). The stress acting on a plane of weakness (e.g. a cleavage plane) in a mineral will be different from the remote loading stresses in the rock, and it is described by the stress intensity factor, K. For a two-dimensional crack, $K = Y(\pi c)^{0.5}\sigma_r$ where Y is a factor related to crack geometry, c is the half-length of the crack and σ_r is the remote stress (Atkinson, 1987). Table 1 shows values of K (MPa $m^{1/2}$) for different cleavage directions in feldspar and quartz. Feldspar has lower K values compared to quartz, except for basal slip (0001) on quartz, which is similar to that of feldspar. In the brittle field where both quartz and feldspar behave in a brittle mode (e.g. sub-greenschist facies), feldspar would be expected to show a higher density of fractures on cleavage planes compared to quartz, and this is observed (e.g. Evans, 1990). Under greenschist conditions, co-existing quartz commonly undergoes grain-size reduction by syn-tectonic recrystallization (Fig. 3a, b, c) or otherwise shows evidence for crystal plastic mechanisms of deformation. The intimate association of plastically deformed quartz within the phyllonite fabric indicates that the micas formed under similar temperature and strain rate conditions as quartz. Oxygen isotopic fractionations between recrystallized quartz and feldspar grains in the mylonites yield temperatures of deformation in the range 325–400 °C (O'Hara et al., 1997).

The brittle deformation of feldspar is likely to have two important consequences in phyllonites. First, grain-size reduction will result in increased reaction rate as the surface area increases, and second, brittle failure will enhance rock permeability and further promote fluid–rock reaction.

4. Chemical reactions in phyllonites

Reaction weakening in phyllonites has been addressed by several authors (Dixon and Williams, 1983; O'Hara, 1988; Wintsch et al., 1995; Hippertt and Massucatto, 1998; Gueydan et al., 2003; Wibberley, 2005; O'Hara, in press). An important weakening reaction common in phyllonites is the breakdown of alkali feldspar to muscovite (Bryant, 1966).

$$\underset{\text{K-feldspar}}{3/2KAlSi_3O_8} + HCl = \underset{\text{Muscovite}}{1/2KAl_3(Si_3Al_3O_{10})(OH)_2} + 3SiO_2 + KCl \quad (1)$$

Fig. 4 shows the stability fields of muscovite and kaolinite relative to K-feldspar as a function of temperature and fluid composition (Hemley, 1959). Also shown are the fields where quartz and feldspar are expected to behave in a brittle versus crystal plastic fashion, resulting in fields labeled *cataclasite* (<300 °C) and *phyllonite* (>300 °C). Based on molar volumes this reaction results in a volume decrease of ~50% when

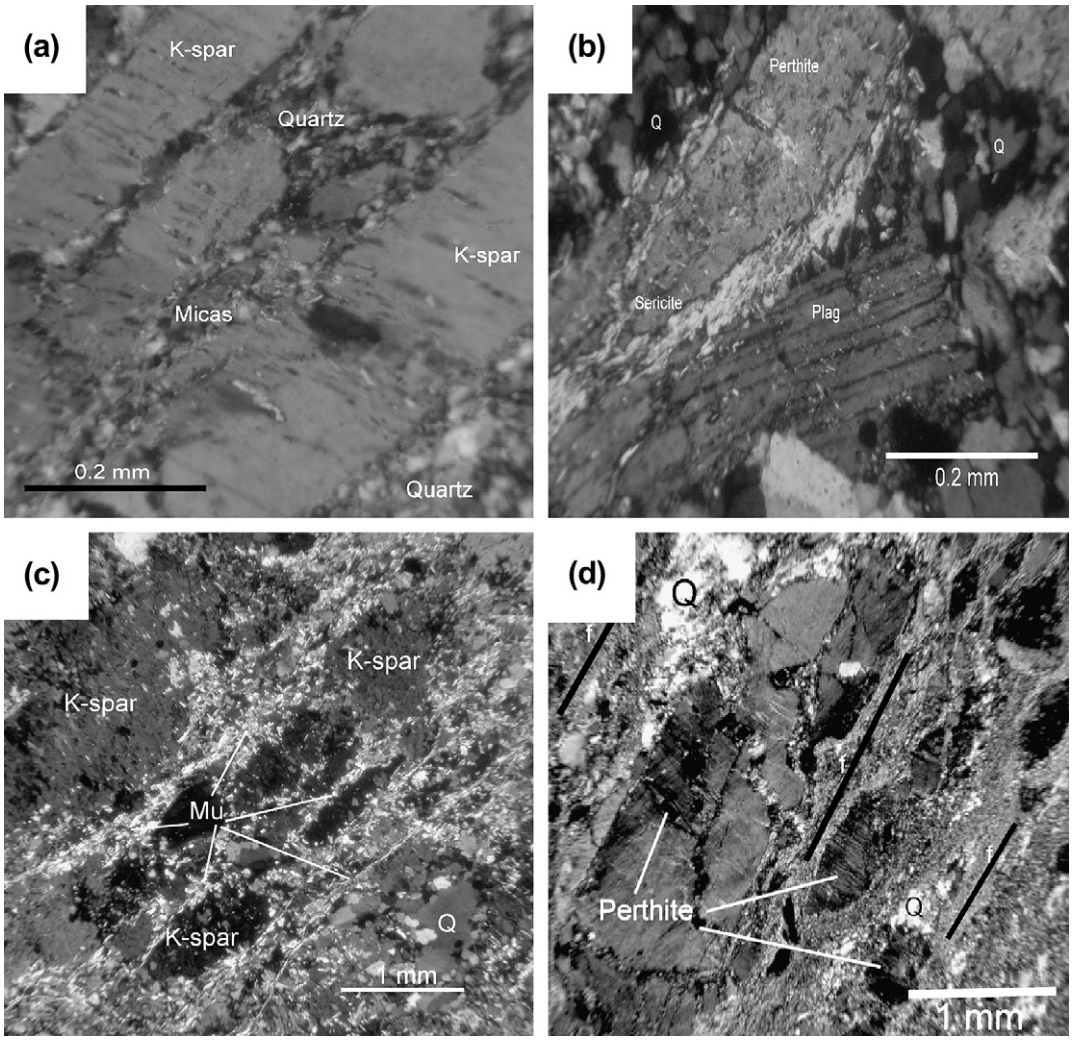

Fig. 3. (a) Rectangular fragments of alkali feldspar in a matrix of recrystallized quartz and minor white mica. Fries thrust, Virginia. Scale bar 0.2 mm. (b) Fragments of perthite and albite showing alteration to white mica (phengite) along margins. K-feldspar shows more alteration compared to albite. Matrix consists of recrystallized quartz (Q). Rector Branch thrust, North Carolina. Scale bar 0.2 mm. (c) Breakdown of alkali feldspar grains to fine-grained muscovite (Mu). A muscovite-rich foliation is developed between feldspar and quartz grains. Quartz shows recrystallization to a finer grain size. Rector Branch thrust. Scale bar 1 mm. (d) Phyllonite showing strong muscovite-rich foliation (black lines) between feldspar-rich zones. Feldspars show elliptical shapes, reflecting dissolution. Quartz (Q) is recrystallized and is part of the mylonitic fabric. Rector Branch thrust. Scale bar 1 mm.

aqueous quartz is removed in solution in an open system (O'Hara, 1994). Wibberley (1999) suggested that in cases where silica is not removed in the fluid phase, but rather precipitates as a cement, this reaction may cause reaction *hardening*. On the basis of volume loss observed in these rocks, it is likely that silica was removed in the fluid.

Fig. 4 shows that muscovite can be stabilized relative to feldspar by two end-member paths: (1) a decrease in temperature at constant fluid composition (path $a-b$) and (2) a decrease in the mKCl/mHCl ratio (increased acidity) at constant temperature (path $d-c$). For example, at about 350 °C, influx of a fluid with a mKCl/mHCl ratio less than about 10^3 would cause dissolution of feldspar and precipitation of muscovite. In the case of path $a-b$, given the presence of a pervasive fluid, the rate of reaction will be controlled by mineral surface reaction and also by the amount of undercooling. In the case of path $d-c$, the rate of reaction maybe controlled by either surface reaction or transport of fluid to the site of reaction (e.g. Lasaga, 1997). Walther and Wood (1984) have emphasized the rapid rate of metamorphic reactions in general, suggesting that diffusion control maybe dominant under metamorphic conditions. On the other hand, more recent diffusion measurements in mica-rich mylonites indicate surprisingly rapid diffusion rates (Farver and Yund, 1999). Below, a model is presented in order to evaluate the relative

Table 1
Stress intensity factor K on selected cleavage planes[a]

Alkali feldspar	Quartz
0.39 (001)	0.31 (0001)
0.39 (010)	0.85 (normal to r)
0.31 (110)	1.0 (normal to z)

[a] Atkinson and Meredith (1987).

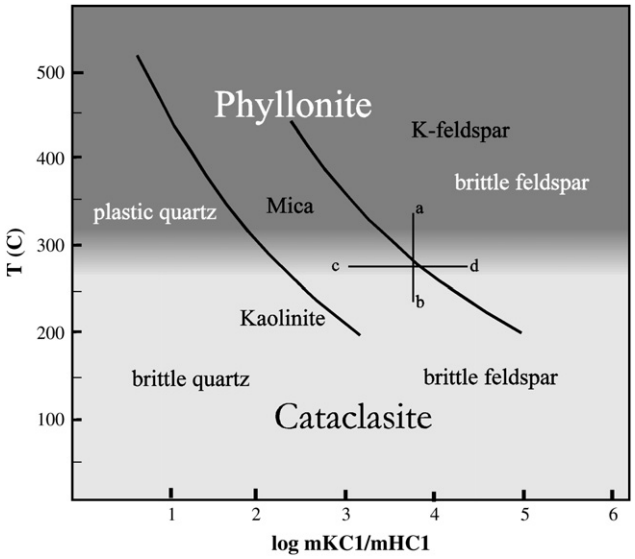

Fig. 4. Plot of temperature versus fluid composition showing stability fields of K-feldspar, muscovite and kaolinite (Hemley, 1959). The molal ratio mKCl/mHCl controls the alteration of alkali feldspar to muscovite at a given temperature (e.g. path *d*–*c*). Breakdown of alkali feldspar to muscovite can also be produced by a decrease in temperature at constant mKCl/mHCl (path *a*–*b*). The phyllonite field (shaded region) includes mica-rich mylonites where quartz behaves plastically, and feldspar behaves in a brittle mode. The cataclasite field includes mica and clay-rich fault rocks in which both feldspar and quartz are brittle.

importance of diffusion versus reaction rate in the formation of the phyllonites, within the context of the Blue Ridge province.

5. Fluid transport and deformation models

5.1. Fluid transport model

In the western Blue Ridge province westward emplacement of crystalline thrust sheets took place during the middle and late Paleozoic onto Late Precambrian clastic sedimentary rocks and Paleozoic carbonates (Goldberg and Dallmeyer, 1997; Hatcher et al., 2005). Oxygen and hydrogen isotope analyses of minerals in the mylonites are consistent with derivation of the fluids from the underlying Paleozoic carbonate and Late Precambrian clastic sedimentary rocks (O'Hara et al., 1995). Fluid inclusion studies indicate that the fluids were NaCl–$CaCl_2$ brines with variable salinities (5–25 wt% NaCl equivalent; O'Hara et al., 1995).

The model involves two scales of fluid transport (Fig. 5). Large scale fluid flow (solid arrows) occurs on fractures, solution features (in Paleozoic carbonates) or faults that supply fluid from the footwall to the base of the thrust. In the case of phyllonites developed between basement slices (e.g. Fries thrust; O'Hara, 1990), it is inferred that fluid must have gained access to the fault through fractures in the basement. Fluid flow also occurs parallel to the thrust zone. The driving force of fluid flow is provided by the lithostatic load of the thrust sheet. Transport on a smaller scale is by solute diffusion in the pore fluid (open arrows) into the base of the thrust sheet, accompanied by simultaneous chemical reaction at the mineral–fluid interface (double headed arrows).

5.2. Grain-scale deformation model

Based on the brittle behavior of feldspar described above (e.g. Fig. 3) a deformation model is suggested in which feldspar grains undergo simple shear (plane strain) along a fracture (cleavage) plane. The displacement corresponds to the horizontal dimension of the grain, resulting in two grains with half the initial height (Fig. 6b). The process is repeated until the feldspar is dissolved by chemical reaction. That the displacement corresponds to the grain dimension is somewhat arbitrary, but it is a convenient minimum unit on which to calculate reaction progress during each strain increment. This simple model may be more appropriate at high strains, where the shear surfaces become sub-parallel to the shear direction with increasing strain (e.g. Fig. 3d).

Starting with a cube of feldspar with a dimension of 1 cm (Fig. 6a), after the first increment of simple shear, the surface area of the two new half-height feldspar grains is 8 cm^2 (Fig. 6b). After the second step the total surface area of four quarter-height grains is 12 cm^2 (Fig. 6c) and after the third step (not shown) it is 20 cm^2. By induction, the total surface area at any given step is $S = (4/2^n + 2)2^n$, but the amount of *new* feldspar surface at each step is simply $S_{new} = 2^n$. Because feldspar is dissolving the new heights of the grains will be somewhat less than illustrated.

A shear strain of $\gamma = 1$ is produced as a result of the first ($n = 1$) strain increment (Fig. 6b). Shear strain in subsequent increments is given by $\gamma = 2^n (n > 1)$. In the model, each increment of strain is only allowed to occur after each new grain is coated with a thin layer of mica according to Eq. (1) above. Solute must first diffuse along the fracture or cleavage plane in order for reaction to take place on that plane. The shear strain is controlled by either the feldspar dissolution rate or the fluid transport rate, whichever is *slowest*. A minimum critical shear stress of 20 MPa is assumed before slip can occur (Mariani et al., 2006).

Although a differential stress is required in order for slip to occur, there is no implication in the present model that feldspar dissolution occurs by pressure solution. Pressure solution involves enhanced dissolution under non-hydrostatic stress conditions (e.g. Green, 1984). In the current model, feldspar dissolution occurs solely because it is outside its stability field under hydrostatic conditions (Fig. 4). In the following section the deformation model is combined with the kinetics of Eq. (1) to provide a temporal model for the evolution of the phyllonite fabric.

6. Kinetics

6.1. Mineral surface reaction

Under the provisional assumption that diffusive transport is sufficiently rapid, the reaction will be controlled by the

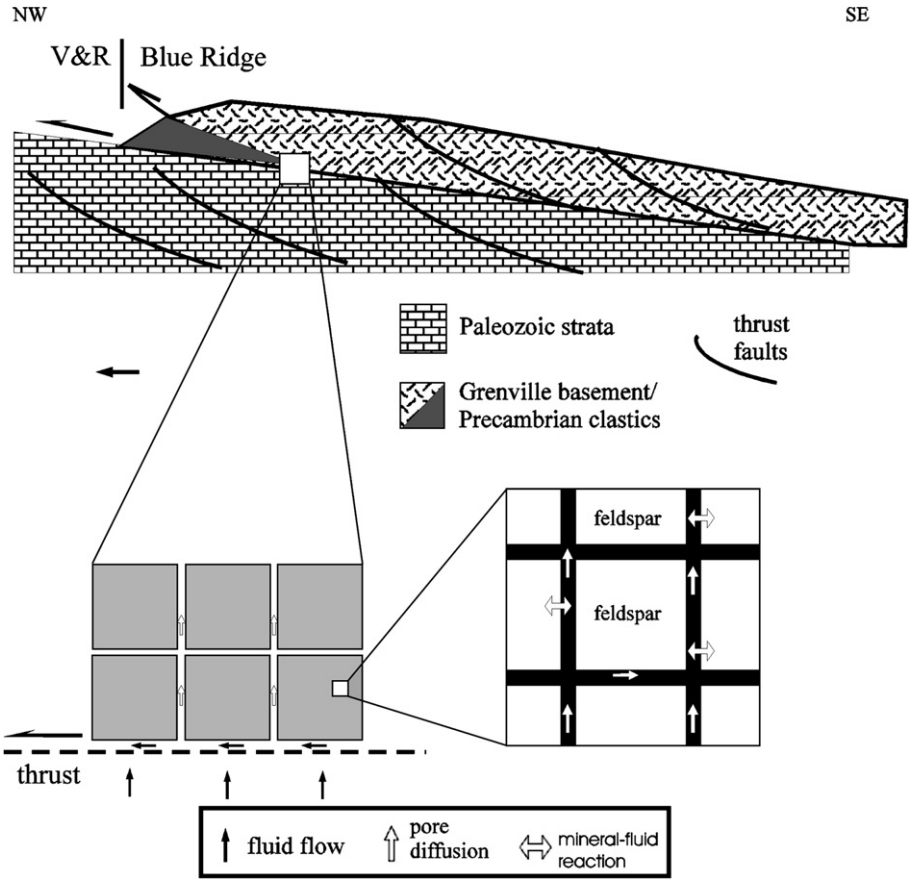

Fig. 5. Fluid transport model for Blue Ridge thrust zone. Fluid flow (solid arrows) occurs along faults, joints or fractures in the footwall rocks. Transport into the shear zone occurs by diffusion (inset, open arrows) and surface-mineral reaction is indicated by double headed arrows. Depending on the relative rates of surface reaction and diffusion the rate of reaction will be either diffusion controlled (fast reaction) or surface reaction controlled (fast diffusion). V&R = Valley and Ridge province. Figure not to scale.

mineral–fluid interface, and the rate of the dissolution reaction can be expressed as (Walther and Wood, 1984; Lasaga, 1997)

$$\frac{dm}{dt} = k_r\left[1 - \exp\left(\frac{\Delta G_r}{RT}\right)\right] \quad (2)$$

where dm/dt is the net observable rate of reaction, k_r is a rate constant, ΔG_r is the Gibbs free energy for the overall reaction and T is absolute temperature and R is the gas constant. Depending on the value of $\Delta G_r/RT$, a useful approximation can be made. If $\Delta G/RT$ is large enough and negative, then Eq. (2) simplifies to

$$\frac{dm}{dt} = k_r \quad (3)$$

In general, Eq. (3) is a good approximation for $\Delta G_r/RT$ values less than −6.

Based on experimentally determined equilibrium constants, Hemley (1959) provided estimates of ΔG for this reaction at different temperatures (Table 2). The Gibbs free energy for feldspar alteration increases with decreasing temperature so that the reaction is promoted under retrograde conditions. The value of $\Delta G/RT$ becomes more negative at lower temperatures and for temperatures <400 °C it is less than −6, the condition where the simple linear reaction rate above ($dm/dt = k_r$) is a good approximation.

Taking into account the effect of mineral surface area on reaction rate (Lasaga, 1997; Walther and Wood, 1984), Eq. (3) is rewritten as

$$\frac{dm}{dt} = k_r S \quad (4)$$

where dm/dt is in moles/cm^3/s, k_r is in moles/cm^2/s and S is the mineral surface area (cm^2/cm^3). Based on previously published experimental data, Wood and Walther (1983) proposed a "master" equation for k_r over a large temperature range under near neutral pH conditions for all silicates

$$\log k_r = \frac{-2900}{T} - 6.85 \quad (5)$$

where k is now in number of gram atoms of oxygen per mole. In the context of Eq. (1) above, feldspar has 8 g oxygen per mole so that Eq. (5) can be converted to moles by dividing by 8. Taking the logarithm of both sides of Eq. (4) and substituting in Eq. (5), gives

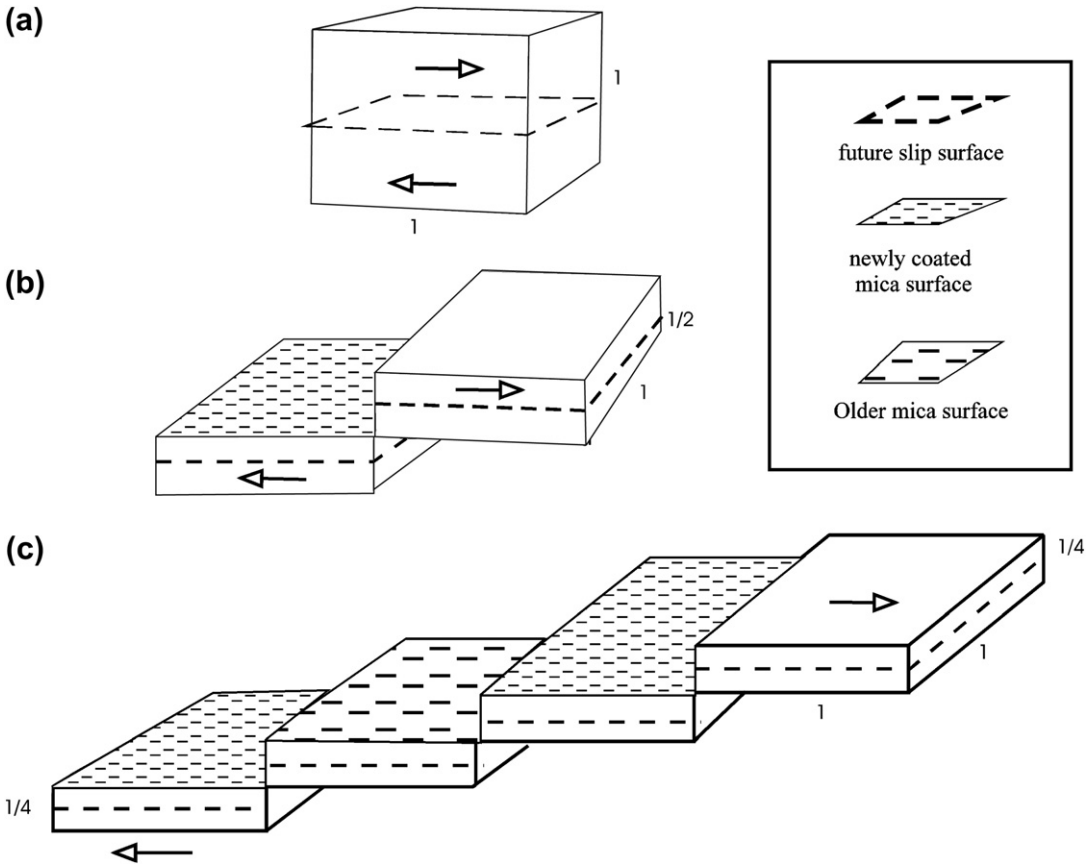

Fig. 6. Model of feldspar deformation showing three stages of grain-size reduction by simple shear along planes of weakness (cleavages). (a) The initial cubic grain has a dimension of 1 cm and a surface area of 6 cm^2. (b) Two new grains with height approximately half the original grain are produced for $n = 1$, with a total surface area of 8 cm^2. (c) For $n = 2$, the total surface area of four quarter-height grains is 12 cm^2. For $n = 3$ (not shown) the total surface area is 20 cm^2. The amount of additional *new* surface area exposed in each increment is given by $S_{new} = 2^n$ ($n > 0$). The shear strain after the first increment is $\gamma = 1$. In subsequent increments ($n > 1$) $\gamma = 2^n$.

$$\log\left(\frac{dm}{dt}\right) = \frac{-2900}{T} - 6.85 - \log n + \log S \quad (6)$$

where n (=8) is the number of gram atoms of oxygen per mole. A potential problem with the application of Eq. (5) above is that the nucleation of one of the product phases may control reaction rate. The common presence of mica, even in weakly deformed phyllonites (e.g. Fig. 3a), suggests, however, that nucleation of this phase is not rate controlling.

In the deformation model (Fig. 6) each increment of strain occurs after each feldspar grain is coated with mica according to Eq. (1) above. The system is open and the model therefore allows for volume loss, which is thought to be important in this rock type (O'Hara, 1994). The volume of mica required to coat feldspar at any given step is hS_{new}, where h is the thickness of the mica coating and S_{new} is the newly exposed mineral surface. Based on thin section observations (e.g. Fig. 3b) a value of $h = 0.01–0.1$ mm is indicated, but as shown below, the overall conclusion is not sensitive to this value. After a feldspar surface is coated with mica it is assumed that no further reaction takes place on that surface due to the armoring effect of the mica. For a mica density of ρ, the weight of mica at each strain increment is $Sh\rho$. Dividing by the gram molecular weight of muscovite (398.3) gives the number of moles of muscovite, and multiplying by 3 (from the stoichiometry of Eq. (1)) yields the amount of feldspar (in moles) required to be dissolved to produce the coating of muscovite: $m = 0.0075\ h\rho S_{new}$.

Table 2
Thermodynamic quantities at different temperatures for Eq. (1)

T (°C)	200	300	400	500
ΔG (kJ/mol)	−44.4	−38.9	−34.8	−31.0
$\Delta G/RT$	−11.2	−8.2	−6.2	−4.8

The rate of feldspar dissolution (dm/dt) is given by Eq. (6) above. Rearranging and integrating, the time to dissolve m moles of feldspar is given by

$$\log t = \frac{2900}{T} + 6.85 + \log m + \log n - \log S \quad (7)$$

The time required to produce a mica coating on newly created surface area between each strain increment was calculated using Eq. (7). A BASIC routine was used in which surface area, shear strain and time were updated after each strain increment.

Fig. 7 is a plot of total time versus accumulated strain rate at three temperatures (200, 300 and 400 °C) for a mica coating

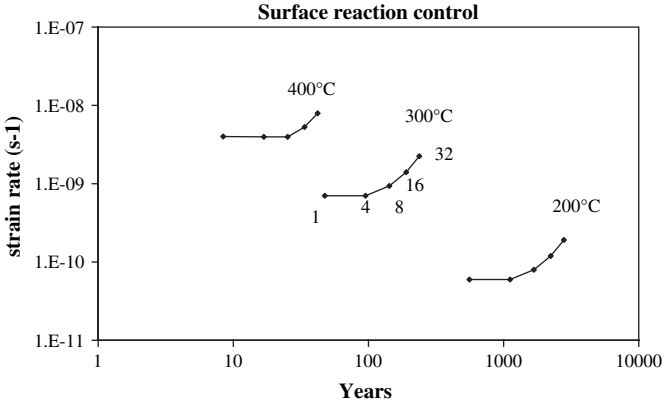

Fig. 7. Plot of strain rate (s^{-1}) versus time (years) for surface reaction control at three different temperatures (200, 300, 400 °C) using Eq. (7). Mica coating thickness = 0.05 mm. Strain rate increases with time due to the geometry of the model ($\gamma = 2^n$, Fig. 6) and also due to increase in surface area. All the feldspar is dissolved after 5 strain increments, corresponding to a shear strain of 32. The strain rates are in the range of 10^{-8} to 10^{-10} s^{-1} between 200 and 400 °C. For complete dissolution of the initial 1 cm^3 grain it takes tens, hundreds and thousands of years at 400, 300 and 200 °C, respectively. The fast dissolution rates indicate surface reaction is not rate controlling.

thickness of 0.05 mm. All of the feldspar is dissolved after five increments of strain. Decreasing the thickness of the mica coating increases the number of dissolution steps, and decreases the overall time for dissolution. Increasing the mica thickness reduces the number of dissolution steps but the overall time to dissolve all the feldspar is similar. The increase in strain rate with time is due to the geometry of the kinetic model ($\gamma = 2^n$) and also because the mineral surface area increases with each step, thereby increasing the reaction rate.

The total time involved for dissolution of 1 cm^3 of feldspar is tens of years at 400 °C, hundreds of years at 300 °C and thousands of years at 200 °C, all of which are geologically very rapid. The strain rates involved are also several orders of magnitude faster than typical orogenic strain rates (Pfiffner and Ramsay, 1982). Fig. 7 indicates strain rates of $\sim 10^{-10}$ at 200 °C, 10^{-9} at 300 °C, and 10^{-8} s^{-1} at 400 °C. These rapid strain rates are inconsistent with the crystal plastic behavior of co-existing quartz (Fig. 3), the microstructures of which are expected to occur only at typical geologic strain rates (10^{-12} to 10^{-14} s^{-1}; Paterson and Luan, 1990). The quartz microstructure is an intimate part of the overall phyllonite fabric and must have formed approximately at the same time. This suggests that surface reaction is not rate controlling, and that the provisional assumption above, that diffusion is sufficiently rapid, is incorrect.

6.2. Bulk diffusion in a static pore fluid

This section places limits on the value of the diffusion coefficient in a confined static interconnected pore fluid. The rapid reaction rates indicated above imply that the solute concentration in the pore fluid near the dissolving feldspar will be the equilibrium value C_{eq}. Away from the mineral surface, the concentration in the pore fluid will correspond to the bulk value C_{bulk}. The driving force for diffusion is the concentration gradient, and by Fick's first law $F = -D(C_{eq} - C_{bulk})$ or $F = -D\partial C/\partial x$, where F is the flux (e.g. g/cm^2/s).

A likely minimum value for diffusion in the mylonites is provided by measured bulk diffusion rates in a mica-rich ultramylonite over the temperature range 250–550 °C at 100 MPa water pressure (Farver and Yund, 1999). In these experiments the diffusion rates parallel to the foliation yield D values of 10^{-14}, 5×10^{-14} and 10^{-13} m^2/s at 200, 300 and 400 °C, respectively. The low activation energy of 30 ± 6 kJ/mol is consistent with the diffusion in stationary water, so that the transport mechanism is inferred to be diffusion in the mylonite through an interconnected static pore fluid along grain boundaries. In the case of diffusive transport in a contact metamorphic aureole, Nagy and Parmentier (1982) modeled a meter-scale exchange of oxygen isotopes using a diffusion coefficient of $\sim 10^{-13}$ m^2/s, which is similar to the experimentally determined values. Microcracks or other high permeability fracture pathways were not thought to be important in the transport properties of the experimental ultramylonite, but such pathways are clearly important in the natural mylonites described above (Fig. 3). The experimental values are therefore likely minimum estimates.

A likely maximum value for the diffusion coefficient in the mylonites corresponds to tracer diffusion (D_t) in unconfined static water. Diffusion in a porous rock under pressure, however, will be slower than an unconfined fluid and tracer diffusion rates in water need to be multiplied by a geometric factor (ω) related to the diffusion porosity (ϕ) and tortuosity (τ) (Neretnieks, 1980). Experimental results indicate that diffusion porosity is a small percentage of the total porosity in granite (Norton and Knapp, 1977). Tortuosity relates to the component of the diffusion path length that is not in the same direction as the concentration gradient (or main diffusion direction). Under these circumstances, the effective diffusivity is reduced by $1/\tau^2$ (van Brakel and Heertjes, 1974). The effective diffusivity D_{eff} can be expressed as

$$D_{eff} = \omega D_t \tag{8}$$

where $\omega = \phi/\tau^2$ is a geometric factor.

The microstructures in Fig. 3 can be used to place some constraints on the porosity. The fracture porosity can be estimated from the fracture length per unit area in the feldspars (~ 1 mm/mm^2), times the fracture width (0.01 mm; Fig. 3), giving $\phi = 10^{-2}$. The fracture width of 0.01 mm is based on the thickness of mica along fractures in feldspar, and is thought to represent the width of the fractures at the P–T conditions of the reaction. The estimated value of ϕ represents a maximum value since the fractures may not be fully interconnected, which would produce porosity "dead-ends". If the fractures are fully interconnected, tortuosity will be low (~ 1) and the geometric factor would correspond to the porosity. In the context of percolation theory (O'Hara, 1994), a large number of dead-end clusters exist at, or close to, the percolation threshold. Under these circumstances the value of τ will be large because the diffusing species must follow a longer

diffusion path. Based on experimental and theoretical considerations, the value for τ ranges from $\sqrt{2}$ to $\sqrt{3}$, being higher in heterogeneous and anisotropic media (van Brakel and Heertjes, 1974). Using the larger value, the geometric factor is then $\omega = 10^{-2}/3$ or 3.3×10^{-3}. In a study of diffusion in intact granitic rocks, Neretnieks (1980) summarized experimental data on rocks up to 50 MPa to suggest a geometric factor of $\sim 10^{-4}$. This is taken as a minimum value since under dynamic conditions (active faulting), dilatancy would cause permeability to increase compared to static conditions (Fischer and Paterson, 1989). The likely range for the geometric factor is therefore estimated to be 10^{-2} to 10^{-4}.

Based largely on electrical conductances of ions in solution, values of aqueous tracer diffusion coefficients are provided by Oelkers and Helgeson (1988) over a range of temperature and pressure. For example, diffusion coefficients for K^+, Na^+ and Cl^{-1} are similar, and yield values of $D_t = 10^{-8}$, 2×10^{-8} and 3×10^{-8} m^2/s at 200, 300 and 400 °C (and 3 kbar), respectively (Oelkers and Helgeson, 1988). The Stokes–Einstein equation considers diffusion of a spherical solute in a dilute solution and expresses diffusion as a function of temperature in a convenient functional form (Lasaga, 1997)

$$D_t = \frac{kT}{6\pi\eta r} \tag{9}$$

where k is Boltzmann's constant, T is temperature (K), η is viscosity of water (Pa s) and r is the atomic radius (m) of the diffusing species. Substituting Eq. (9) into Eq. (8) gives an effective diffusion coefficient

$$D_{\text{eff}} = \frac{\omega kT}{6\pi\eta r} \tag{10}$$

Using the relation $t = x^2/4D_{\text{eff}}$, where t is time, x is distance, a length scale needs to be chosen in order to evaluate the time scale over which diffusion is important. Several phyllonite zones have been described in the southern Appalachians (Sinha et al., 1988; O'Hara, 1988, 1990; Bailey, 1995; Newman and Mitra, 1993) whereby crystalline thrusts are emplaced along phyllonite zones. The thickness of these zones is in the range of 1 to ~100 m. In the context of the model in Fig. 5, this would represent the distance over which a packet of fluid would diffuse from a fracture zone into the matrix of the shear zone. Although mica-rich high strain zones apparently greater than 1 km in thickness are present in the Blue Ridge province, these zones appear to be composite. Mapping at a scale of 1:24,000 indicates that these wide zones are composed of several thinner strands of ~100 m thick that anastomose between less deformed rock (Cattanach and Merschat, 2005).

Under diffusion controlled conditions, the model requires that a time interval t must elapse between each increment of strain, corresponding to the time needed for the diffusing species to travel the diffusion distance ($t = x^2/4D_{\text{eff}}$). The shear strain is given by $\gamma = 2^n$, where n is the strain increment counter. The shear strain rate $d\gamma/d\tau$ is given by $2^n/t$ and substituting in the relation $t = x^2/4D_{\text{eff}}$

$$\frac{d\gamma}{d\tau} = \frac{2^n 4D_{\text{eff}}}{x^2} \tag{11}$$

Substituting Eq. (10) into Eq. (11) gives approximately

$$\frac{d\gamma}{d\tau} = \frac{2^n \omega kT}{5\eta r x^2} \tag{12}$$

To evaluate Eq. (12) the following values are used: $n = 1$–5; $\omega = 10^{-2}$, 3.3×10^{-3} and 10^{-4}; $k = 1.4 \times 10^{-23}$ J/K; $\eta = 10^{-4}$ Pa s; $r = 1.5 \times 10^{-10}$ m and x (shear zone thickness) = 100, 10 and 1 m. The atomic radius used is typical of ions such as Na^+, K^+ and Cl^{-1} (Emsley, 1998) and the viscosity of water at 300 °C and 3 kb is used (Dudziak and Franck, 1966). The resulting diffusion coefficients are similar to those in Oelkers and Helgeson (1988) within ±50%. This error is not sufficient to affect the conclusions. Low values of n can be related to proto-mylonite microstructures with high feldspar contents (e.g. Fig. 2b), whereas high values of n would correspond to ultramylonites, where feldspar is nearly totally dissolved (e.g. Fig. 2d).

Fig. 8a is a plot of strain rate versus time for three temperatures (200, 300, and 400 °C) for $x = 100$ m and $\omega = 3.3 \times 10^{-3}$, based on Eq. (12). Strain rates are typically 10^{-14} to 10^{-13} s^{-1} over this temperature interval, involving times of ~5.5 Ma. The diffusion coefficients range from 1.1×10^{-10} to 7.7×10^{-11} m^2/s and show a weak temperature dependence. The strain rates and times are plausible for an active mountain belt (Pfiffner and Ramsay, 1982) and consistent with the co-existing plastically deformed and recrystallized quartz (Paterson and Luan, 1990). The lower temperature value of 200 °C is more applicable to cataclasites rather than mylonites, where quartz behaves in a brittle or semi-brittle fashion (Fig. 4).

Strain rate increases with time indicating the shear zone is strain weakening. This is due to the increase in reaction rate with grain-size reduction, and also because shear strain is given by a power law ($\gamma = 2^n$). This should lead to the strain localization commonly observed in natural shear zones. As in the case of reaction control above, maximum shear strain is 32, after which all feldspar is dissolved, but there is no reason the zone cannot continue to deform along the mica-rich foliation. Mylonites in which all the feldspar has been dissolved have been reported by several workers in different regions (e.g. Bryant, 1966; Hippertt and Massucatto, 1998; Wibberley, 2005).

Fig. 8b shows a plot of strain rate versus time for three different geometric factors, $\omega_1 = 10^{-2}$, $\omega_2 = 3.3 \times 10^{-3}$ and $\omega_3 = 10^{-4}$ and $x = 100$ m as before. The value of ω has a major effect on the diffusion coefficient and hence reaction time. The diffusion coefficients range from 2.8×10^{-10} to 2.8×10^{-12} m^2/s in these models. The low value of ω_3 (10^{-4}) requires ~100 Ma for substantial reaction, which is clearly unrealistic as erosion would remove the thrust sheet before emplacement was complete. The higher value of ω_2 (3.3×10^{-3}) is the same as in Fig. 8a at 300 °C and yields realistic reaction times and strain rates. The highest value for the

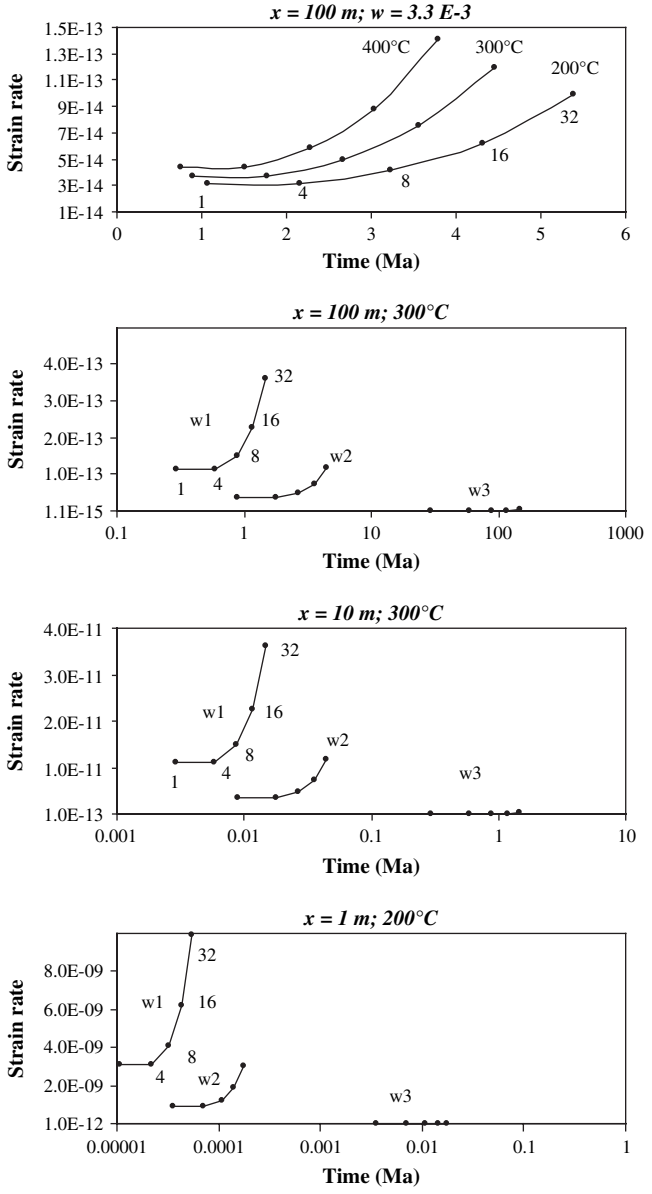

Fig. 8. Plots of strain rate versus time for different temperatures, shear zone widths and geometric factors. Diffusion controlled reaction rates based on Eq. (12) in the text. Data point labels indicate shear strain. (a) Shear zone width = 100 m for three temperatures (200, 300, 400 °C) and a geometric factor of 3.3×10^{-3}. Strain rates range from 10^{-14} to 10^{-13} s^{-1}. The times for reaction are geologically reasonable (1–5 Ma). (b) Shear zone width = 100 m at 300 °C for three different geometric factors $\omega_1 = 10^{-2}$, $\omega_2 = 3.3 \times 10^{-3}$ and $\omega_3 = 10^{-4}$. The resulting strain rates range from 10^{-15} to 10^{-13} s^{-1}. The smallest geometric factor ω_3 yields reaction times that are geologically too long ($\sim$10 Ma). The larger geometric factors ω_1 and ω_2 yield reasonable strain rates and plausible total reaction times. (c) Strain rate versus time for a shear zone width of 10 m at 300 °C for three different geometric factors. The smallest geometric factor ($\omega_3 = 10^{-4}$) yields reasonable reaction times ($\sim$1 Ma) and plausible strain rates (10^{-12}). (d) Shear zone width = 1 m at 200 °C for the three different geometric factors. The smallest geometric factor ($\omega_3 = 10^{-4}$) yields strain rates of $\sim 10^{-12}$ and reaction times of $\sim 10^4$ years. This model may be reasonable in the case of a thin (1 m) diffusion controlled cataclastic shear zone.

geometric factor ($\omega_1 = 10^{-2}$) also yields reasonable strain rates ($\sim 10^{-13}$ s^{-1}) but shorter times (0.2–2 Ma).

Fig. 8c shows a plot of strain rate versus time at 300 °C and the same three values of ω as above, for a shear zone width of $x = 10$ m. The diffusion coefficients have the same range as before (2.8×10^{-10} to 2.8×10^{-12} m^2/s). Strain rates are faster (6×10^{-13} to 1.1×10^{-11} s^{-1}) and deformation times are shorter (2000 years to 1.7 Ma). The lower value of the geometric factor ($\omega_3 = 10^{-4}$) corresponds to a diffusion coefficient of 2.8×10^{-12} m^2/s, a strain rate of 10^{-13} s^{-1} and times of $\sim$2 Ma, all of which appear to be geologically plausible for a relatively narrow (10 m) shear zone.

Fig. 8d shows a plot of strain rate versus time at 200 °C for the three values of ω above and a shear zone width of $x = 1$ m. The diffusion coefficients range from 2.3×10^{-10} to 2.3×10^{-12} m^2/s. The strain rates range from 10^{-8} to 10^{-12} s^{-1} with times of $10–10^4$ years. The slower range in the strain rate (10^{-12}) and the longer times (10^4 years) may be geologically plausible in the case of a minor (1 m), low temperature (cataclastic) shear zone.

Similar modeling of a 1 km wide shear zone indicates that slow strain rates ($<10^{-15}$) and unreasonably long times (>75 Ma) are required, so that a diffusion controlled model has substantial difficulty in explaining such wide zones. As mentioned above, these wide zones appear to be composed of several intertwined narrower shear zones and can be modeled individually on a scale of $\sim 10^2$ m.

In the context of emplacement of orogenic-scale crystalline thrust sheets (e.g. Blue Ridge–Piedmont sheet) the preferred model is that illustrated in Fig. 8a for a 100 m thick shear zone and a geometric factor of 3.3×10^{-3}. This model yields reasonable strain rates and times over a range of temperatures. The relevant diffusion coefficient is $\sim 10^{-10}$ m^2/s. This value is faster than that suggested for diffusion in bedrock related to radionuclide disposal at shallow depths (10^{-12} m^2/s; Neretnieks, 1980) but similar to that suggested for regional metamorphism (e.g. Rubie and Thompson, 1985). It is about three orders of magnitude faster than the rate used to model a meter-scale diffusive exchange zone across a contact metamorphic aureole (Nagy and Parmentier, 1982) and about three to four orders faster than the experimental results in a mica-rich fine-grained homogeneous ultramylonite (Farver and Yund, 1999). The rocks within an actively deforming shear zone, however, are likely to have higher diffusivity pathways compared to a more passive tectonic setting, such as a contact metamorphic aureole, or static experiments on a fine-grained homogeneous ultramylonite.

7. Damkohler number

The conclusion that diffusion is the rate limiting transport mechanism is reinforced by estimating the dimensionless Damkohler number (Da), which is the ratio of the chemical reaction rate to the diffusion rate. For Da numbers $\gg 1$, reaction rates dominate, and diffusion is rate controlling (Lasaga, 1997)

$$Da = \frac{k_{\text{eff}} L^2}{D_{\text{eff}}} \tag{13}$$

where the effective reaction rate $k_{\text{eff}} = (A/\phi)(k_r/C_{\text{eq}})$, and A is the mineral surface area per unit volume of pore fluid, ϕ is

porosity, k_r is the dissolution rate and C_{eq} is the concentration in the fluid; k_{eff} has units of s^{-1}. D_{eff} is the effective diffusion coefficient and L is the diffusion length scale. Taking the following values: $A = 6\ cm^2/cm^3$, $\phi = 10^{-2}$, $k_r = 10^{-12}$ moles/cm^2/s at 300 °C (Eq. (5)), C_{eq} for silica at 300 °C = 7×10^{-6} moles/cm^3 of fluid, $D_{eff} = 10^{-6}\ cm^2/s$ and $L = 1$ cm, yields a value for Da of 10^2. Diffusion therefore is rate limiting, even on a centimeter scale. A larger surface area (i.e. smaller grains) and longer diffusion distances only strengthen this conclusion. To negate this conclusion, the diffusion coefficient would have to be the same as that in an unconfined static fluid (i.e. two orders of magnitude faster), which is implausible.

This result is consistent with the conclusion of Walther and Wood (1984) and Knapp (1989) that reaction rates at elevated temperatures are in general diffusion controlled. In contrast, Gueydan et al. (2003) implicitly assume reaction kinetics are the rate controlling mechanism in their deformation–reaction model. Their results allow phyllonite shear zones up to 4 km wide to develop in 0.5 Ma, which is substantially faster than the diffusion controlled model in this study. The model of Niemeijer and Spiers (2005), as applied to crustal strength profiles, also assumes a reaction-controlled rheology. The diffusion controlled model proposed here successfully predicts geologic strain rates under greenschist conditions on a scale of 10–100 m. The model can be applied to other tectonic settings where crystalline thrust sheets are emplaced along phyllonite shear zones under greenschist conditions (e.g. the Alps and the Caledonides; Wibberley, 2005), and also to crustal-scale strike slip faults (e.g. Median Tectonic Line, Japan; Jefferies et al., 2006).

8. Tectonic implications

8.1. Rheology

It has been recognized for some time that in the frictional regime micas and clays are weak compared to other rock types (Byerlee, 1978), possibly because micas can deform by dislocation glide over a wide range of temperature and strain rate conditions (Kronenberg et al., 1990). Mica-rich rocks with a substantial component of feldspar and quartz, however, are likely to be stronger than single crystals (Shea and Kronenberg, 1992). In cases where mica-rich rocks have a well-developed foliation, however, strengths may be as low as 10 MPa (Wintsch et al., 1995). More recent shear experiments on muscovite also indicate that at low experimental strain rates and high temperatures, dramatic weakening occurs during viscous flow of mica (1–10 MPa; Mariani et al., 2006). The presence of crystal plastic deformation microstructures in quartz coexisting with retrograde mica, suggests that extrapolation of quartz flow laws can place additional constraints on the strength of the natural phyllonites. Extrapolation of quartz rheologies to strain rates of $10^{-14}\ s^{-1}$ indicates strengths in the approximate range of 10–100 MPa (Paterson and Luan, 1990). The weakness of the mica-rich foliation in these rocks would favor the lower strength estimate.

The rheologies for intracrystalline plasticity and that for phyllonite proposed here are very different. The flow law for intracrystalline plasticity (dislocation creep) usually takes the form $de/dt = A\sigma^n \exp(-Q/RT)$, where e is the strain, σ is stress, T is absolute temperature and A, n and Q are constants. The rate controlling mechanism is volume diffusion in the crystal lattice, which is determined by the activation energy Q (typically ~150 kJ/mol). The exponential dependence of strength on temperature results in rapid weakening over a narrow temperature interval (Carter and Tsenn, 1987).

In contrast, the rheology proposed for phyllonite has the form $d\gamma/dt = 2^n \omega T/\eta r x^2$ where γ is shear strain, n and ω are constants, T is absolute temperature, η is the fluid viscosity, r is the radius of the diffusing species, and x is the diffusion distance. The linear dependence of strain rate on temperature indicates a weaker role for temperature compared to dislocation creep mechanisms. This is also indicated by the lower activation associated with diffusion in a fluid (~20 kJ/mol; Lasaga, 1997). This suggests that formation of the phyllonite can occur over a larger range of temperature conditions compared to quartz plasticity, which requires a minimum temperature, commonly cited to be ~300 °C. Thus, under diffusion controlled conditions, breakdown of feldspar to mica and clays can be expected in both cataclasites and mylonites over a range of metamorphic conditions (200–400 °C; Fig. 4).

Based on experimental evidence, the strength of mica in the phyllonite at mid-crustal conditions is assumed to be ~20 MPa (e.g. Mariani et al., 2006). Below a shear stress of 20 MPa it is assumed that there is no strain, and above 20 MPa the strain rate follows a modified Stokes–Einstein relation

$$\frac{d\gamma}{dt} = 0 \quad < 20\ \text{MPa} \tag{14a}$$

$$\frac{d\gamma}{dt} = \frac{2^n \omega k T}{5 \eta r x^2} \quad > 20\ \text{MPa} \tag{14b}$$

8.2. Initial detachment

Foreland fold and thrust belts are common features of orogenic belts involving brittle thrust emplacement usually along weak detachment surfaces (e.g. shale or evaporite). In the case of crystalline thrusts, however, weak lithologies do not exist, and understanding the development of high strain zones along their base has been problematic. Previous workers (e.g. Armstrong and Dick, 1974) have suggested that these crystalline thrusts became detached from their source at the brittle–ductile transition in the crust, corresponding to the onset of ductile behavior of quartz. The ubiquitous presence of phyllonites at the base of the Blue Ridge thrust sheets suggests an alternative mechanism, namely reaction weakening due to syn-tectonic mica production. Chemical reaction can explain continued weakness after thrust emplacement, but a mechanism is required to explain

how these thrust slices *initially* become detached from their basement source.

In common with most orogenic belts, an earlier rifting event preceded the emplacement of crystalline thrusts in the southern Appalachians. Seismic studies show that steep normal faults are common in the basement rocks, and detailed geologic studies indicate that thrusting in some cases followed pre-existing normal faulting in the Appalachians (Simpson and Kalaghan, 1989) and the Alps (Wibberley, 2005). This earlier normal faulting would "pre-condition" the basement by fracturing, thereby allowing infiltration of water to promote retrogression and weakening. It is suggested that initial detachment during subsequent compression is promoted by this earlier faulting and fracturing of the basement.

Fig. 9a shows a passive continental margin after a rifting event, with normal faults offsetting the basement rocks. During subsequent compression, these damage zones become infiltrated by pore fluid along a fracture network and promote retrograde chemical reaction, leading to weakening (Fig. 9b). Strain weakening leads to strain localization along sole thrusts, and basement slices become detached from their source (Fig. 9c). Thrust emplacement is inferred to be in a break forward sequence, with deeper thrusts forming later (Goldberg and Dallmeyer, 1997). The source of fluid after initial thrust detachment is likely to be from the Paleozoic carbonate or Precambrian clastic sedimentary and meta-sedimentary rocks onto which the thrust sheets were emplaced (O'Hara et al., 1995).

9. Conclusions

A deformation model involving brittle grain-size reduction of feldspar followed by chemical breakdown to mica shows that mineral surface dissolution of feldspar produces unreasonably fast strain rates. It is concluded that the rate limiting step is transport by diffusion in an interconnected fracture-dominated porosity with a diffusion coefficient in the range $\sim 10^{-10}$ to 10^{-12} m^2/s over the approximate temperature interval 200–400 °C. This corresponds to a depth interval of 8–16 km, assuming a geotherm of 25 °C/km. The model produces strain rates of $\sim 10^{-13}$ to 10^{-14} s^{-1} (for a diffusion distances of 10–100 m) which are geologically plausible and also consistent with co-existing quartz microstructures at these strain rates. Based on experimental studies for the strength of micas and quartz, and their coexistence in the phyllonites, the shear strength is estimated to be ~20 MPa at geologic strain rates over the depth interval 8–16 km. The linear dependence of

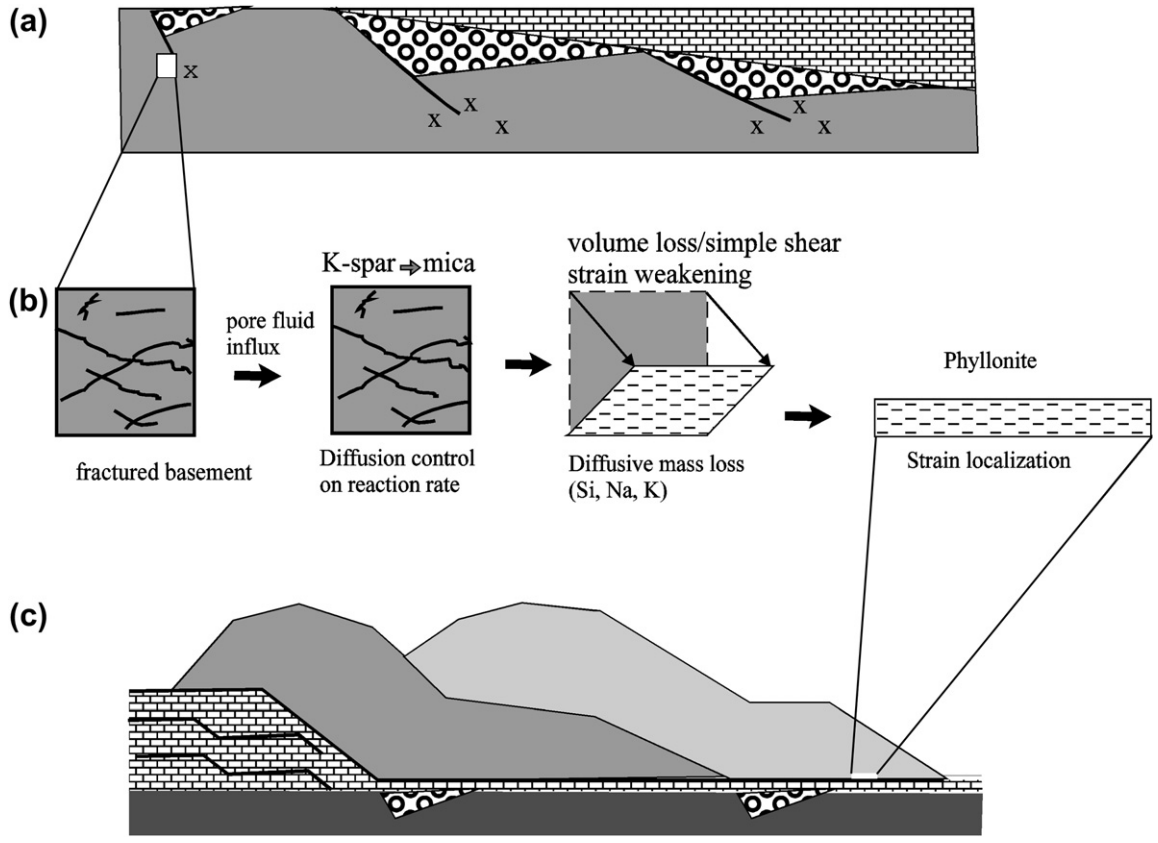

Fig. 9. (a) Schematic drawing of a passive continental margin showing normal faults in the basement. X's mark the sites of likely fracture damage, where fluid infiltration into the basement rock is inferred to occur. (b) Sequential development of phyllonite during a compressional phase. Fluid infiltration into the basement rocks causes reaction weakening. Diffusive mass transfer results in volume loss during non-coaxial shear. Strain weakening leads to strain localization, and basement slices become detached from the continental edge. (c) Once a basement slice becomes detached from its source, it is emplaced along basal phyllonite zones. Fluid is provided by the sedimentary rocks in the footwall. The strain rate and strength of the detachments are controlled by solute diffusion in the pore fluid and the strength of phyllosilicates. Thrust emplacement is inferred to occur in a break forward sequence. Brick pattern: Paleozoic succession; circle pattern: Late Precambrian clastics; gray shading: crystalline basement.

phyllonite strain rate on temperature suggests that phyllonites can form over a larger range in temperature compared to mylonites produced by crystalline plasticity. If crystalline thrust sheets are emplaced along phyllonite zones they may become detached from their source over a range of depths and not just at a depth corresponding to the brittle–ductile transition as previously suggested. The mechanism of phyllonite formation requires a source of fluid which, on the basis of isotopic analyses and fluid inclusion measurements, is interpreted to be derived from the underlying sedimentary and metasedimentary rocks in the footwall. The kinetic model in this study is also applicable to formation of phyllonites in both strike slip and extensional tectonic settings.

Acknowledgments

Journal reviews by Christopher Wibberley and Christopher Bailey substantially improved the manuscript. Editorial handling by J. Hippertt is also appreciated.

References

Armstrong, R.L., Dick, H.J.B., 1974. A model for the development of thin overthrust sheets of crystalline rock. Geology 1, 35–40.

Atkinson, B.K., 1987. Introduction to fracture mechanics and its geophysical applications. In: Atkinson, B.K. (Ed.), Fracture Mechanics of Rock. Academic Press, pp. 1–23.

Atkinson, B.K., Meredith, P.G., 1987. Experimental fracture mechanics data for rocks and minerals. In: Atkinson, B.K. (Ed.), Fracture Mechanics of Rock. Academic Press, pp. 477–527.

Bailey, C.M., 1995. Heterogeneous strain in granitic mylonites from the Rockfish valley fault, central Virginia. Journal of Geodynamics 19, 177–194.

Boyer, S., Elliott, D., 1982. Thrust systems. American Association of Petroleum Geologists Bulletin 66, 1196–1230.

Brace, W.F., Kohlstedt, D.L., 1980. Limits on lithospheric stress imposed by laboratory experiments. Journal of Geophysical Research 85, 6248–6252.

Bryant, B., 1966. Formation of Phyllonites in the Grandfather Mountain Window Area, Northwestern North Carolina. U.S. Geological Survey Professional Paper 615.

Byerlee, J.D., 1978. Friction of rocks. Pure and Applied Geophysics 116, 615–626.

Carter, N.L., Tsenn, M.C., 1987. Flow properties of continental lithosphere. Tectonophysics 136, 27–63.

Cattanach, B.L., Merschat, C.E., 2005. An overview of the Mesoproterozoic basement complex on the west half of the Ashville 1:100,000 scale geologic map. In: Hatcher Jr., R.D., Merschat, A.J. (Eds.), Blue Ridge Geology Geotraverse East of the Great Smoky Mountains National Park, North Carolina. Carolina Geological Society Annual Field Trip Guide, pp. 25–32.

Cook, F.A., Albough, D.S., Brown, L.D., Kaufman, S., Oliver, J.E., 1979. Thin-skinned tectonics in the crystalline southern Appalachians; COCORP seismic-reflection profiling of the Blue Ridge and Piedmont. Geology 7, 563–567.

Deer, W.A., Howie, R.A., Zussman, J., 1992. An Introduction to the Rock-forming Minerals, second ed. Longman, 696 pp.

Dixon, J., Williams, G., 1983. Reaction softening in mylonites from the Arnaboll thrust, Sutherland. Scottish Journal of Geology 19, 157–168.

Dudziak, K.H., Franck, E.U., 1966. Messungen der viskosität des wassers bis 560 °C und 3500 bar. Berichte der Bunsengesellschaft Phys. Chem. 70, 1120–1128.

Emsley, J., 1998. The Elements, third ed. Oxford Press, 293 pp.

Evans, J.P., 1990. Textures, deformation mechanisms and the role of fluids in the cataclastic deformation of granitic rocks. In: Knipe, R.J., Rutter, E.H. (Eds.), Deformation Mechanisms, Rheology and Tectonics. Geological Society, London, Special Publications, pp. 29–39.

Farver, J.R., Yund, R.A., 1999. Oxygen bulk diffusion measurements and TEM characterization of a natural ultramylonite: implications for fluid transport in mica-bearing rocks. Journal of Metamorphic Geology 17, 669–683.

Fischer, G.J., Paterson, M.S., 1989. Dilatancy during deformation of rocks at high temperatures and pressures. Journal of Geophysical Research 94, 17,607–17,617.

Goldberg, S.A., Dallmeyer, R.D., 1997. Chronology of Paleozoic metamorphism and deformation in the Blue Ridge thrust complex, North Carolina and Tennessee. American Journal of Science 297, 488–526.

Green, H.W., 1984. "Pressure solution" creep: some causes and mechanisms. Journal of Geophysical Research 89, 4313–4318.

Gueydan, F., Leroy, Y.M., Jolivet, L., Agard, P., 2003. Analysis of continental midcrustal strain localization induced by microfracturing and reaction softening. Journal of Geophysical Research 108, doi:10.1029/2001JB000611.

Hatcher Jr., R.D., Merschat, A.J., Thigpen, J.R., 2005. Blue Ridge primer. In: Hatcher Jr., R.D., Merschat, A.J. (Eds.), Blue Ridge Geology Geotraverse East of the Great Smoky Mountains National Park, West North Carolina. Carolina Geological Society Annual Field Trip Guide, pp. 1–24.

Hatcher Jr., R.D., Hooper, R.J., 1992. Evolution of crystalline thrust sheets in the internal parts of mountain belts. In: McClay, K.R. (Ed.), Thrust Tectonics. Chapman and Hall, London, pp. 217–233.

Hemley, J.J., 1959. Some mineralogical equilibria in the system K_2O–Al_2O_3–SiO_2–H_2O. American Journal of Science 257, 241–270.

Hippertt, J.F., Massucatto, A.J., 1998. Phyllonitization and development of kilometer-size extension gashes in a continental-scale strike-slip shear zone, north Goiás, Central Brazil. Journal of Structural Geology 20, 433–445.

Imber, J., Holdsworth, R.E., Butler, C.A., 2001. A reappraisal of the Sibson–Scholz fault zone model: the nature of the frictional to viscous transition along a long-lived crustal scale fault, Outer Hebirdes, Scotland. Tectonics 20, 601–624.

Janecke, S.U., Evans, J.P., 1988. Feldspar-influenced rock rheologies. Geology 16, 1064–1067.

Jefferies, S.P., Holdsworth, R.E., Wibberley, C.A.J., Shimamoto, T., Spiers, C.J., Niemeijer, A.R., Lloyd, G.E., 2006. The nature and importance of phyllonite development in crustal-scale fault cores: an example from the Median Tectonic Line, Japan. Journal of Structural Geology 28, 220–235.

Knapp, R.B., 1989. Spatial and temporal scales of local equilibrium in dynamic fluid–rock systems. Geochimica et Cosmochimica Acta 53, 1955–1964.

Kronenberg, A.K., Kirby, S.H., Pinkston, J., 1990. Basal slip and mechanical anisotropy of biotite. Journal of Geophysical Research 95, 19257–19278.

Lasaga, A.C., 1997. Kinetic Theory in the Earth Sciences. Princeton Series in Geochemistry, New Jersey, 809 pp.

Laubscher, H.P., 1983. Detachment, shear and compression in the Central Alps. In: Hatcher Jr., R.D., Williams, H., Zietz, I. (Eds.), Contributions to the Tectonics and Geophysics of Mountain Chains. Geological Society America Memoir, vol. 158, pp. 191–211.

Mariani, E., Brodie, K.H., Rutter, E.H., 2006. Experimental deformation of muscovite shear zones at high temperatures under hydrothermal conditions and the strength of phyllosilicate-bearing faults in nature. Journal of Structural Geology 28, 1569–1587.

Nagy, K.L., Parmentier, E.M., 1982. Oxygen isotopic exchange at an igneous contact. Earth and Planetary Science Letters 59, 1–10.

Newman, J., Mitra, G., 1993. Lateral variations in mylonite zone thickness as influenced by fluid–rock interactions, Linville Falls fault, North Carolina. Journal of Structural Geology 15, 849–863.

Neretnieks, I., 1980. Diffusion in the rock matrix: an important factor in radionuclide retardation. Journal of Geophysical Research 85, 4379–4397.

Niemeijer, A.R., Spiers, C.P., 2005. Influence of phyllosilicates on fault strength in the brittle–ductile transition: insights from rock analogue experiments. In: Bruhn, D., Burlini, L. (Eds.), High Strain Zones, Structure and Physical Properties. Geological Society, London, Special Publications, vol. 245, pp. 303–327.

Norton, D., Knapp, R., 1977. Transport phenomena in hydrothermal systems: the nature of porosity. American Journal of Science 277, 913–936.

Oelkers, E.H., Helgeson, H.C., 1988. Calculation of the thermodynamic and transport properties of aqueous species at high pressures and temperatures: aqueous tracer diffusion coefficients of ions at 1000 °C and 5 kb. Geochimica et Cosmochimica Acta 52, 63–85.

O'Hara, K., 1988. Fluid flow and volume loss during mylonitization: an origin for phyllonite in an overthrust setting. Tectonophysics 156, 21–34.

O'Hara, K., 1990. State of strain in mylonites from the western Blue Ridge province, southern Appalachians: the role of volume loss. Journal of Structural Geology 12, 419–430.

O'Hara, K., 1994. Fluid–rock interaction in crustal shear zones: a directed percolation approach. Geology 22, 843–846.

O'Hara, K., Kirschner, D.L., Moecher, D.P., 1995. Petrologic constraints on the source of fluid during mylonitization in the Blue Ridge province, North Carolina and Virginia, USA. Journal of Geodynamics 19, 271–287.

O'Hara, K., Sharp, Z.D., Moecher, D.P., Jenkin, G.R., 1997. The effect of deformation on oxygen isotope exchange in quartz and feldspar and the significance of isotopic temperatures in mylonites. Journal of Geology 105, 193–204.

O'Hara, K., in press. Coupled deformation and reaction softening processes: retrograde shear zones in the Rosslare complex, SE Ireland. Irish Journal of Earth Sciences.

Paterson, M.S., Luan, F.C., 1990. Quartzite rheology under geological conditions. In: Knipe, R.J., Rutter, E.H. (Eds.), Deformation Mechanisms, Rheology and Tectonics. Geological Society, London, Special Publications, pp. 299–307.

Pfiffner, O.A., Ramsay, J.G., 1982. Constraints on geological strain rates: arguments from finite strain states of naturally deformed rocks. Journal of Geophysical Research 87, 311–321.

Rast, N., Kohles, K., 1985. In: Woodward, N.B. (Ed.), Valley and Ridge thrust belt: balanced structural sections, Pennsylvania to Alabama. Studies in Geology, vol. 12. Appalachian Basin Industrial Associates, University of Tennessee, p. 38.

Rubie, D.C., Thompson, A.B., 1985. Kinetics of metamorphic reactions at elevated temperatures and pressures: an appraisal of available experimental data. In: Thompson, A.B., Rubie, D.C. (Eds.), Metamorphic Reactions. Advances in Physical Geochemistry 4, 27–71.

Schedl, A., McCabe, G., Montanez, I.P., Fullagar, P.D., Valley, J.W., 1992. Alleghanian regional diagenesis: a response to the migration of modified metamorphic fluids derived from beneath the Blue Ridge-Piedmont thrust sheet. Journal of Geology 100, 339–352.

Shea, W.T., Kronenberg, A.K., 1992. Rheology and deformation mechanisms of an isotropic mica schist. Journal of Geophysical Research 97, 15201–15237.

Simpson, C., Kalaghan, T., 1989. Late Precambrian crustal extension preserved in the Fries fault zone mylonites, southern Appalachians. Geology 17, 148–151.

Sinha, A.K., Hewitt, D.A., Rimstidt, J.D., 1988. Metamorphic petrology and strontium isotope geochemistry associated with the development of mylonites: an example from the Brevard fault zone, North Carolina. American Journal of Science 288, 115–147.

van Brakel, J., Heertjes, P.M., 1974. Analysis of diffusion in macroporous media in terms of a porosity, a tortuosity and a constrictivity factor. International Journal of Heat and Mass Transfer 17, 1093–1103.

Walther, J.V., Wood, B.J., 1984. Rate and mechanism in prograde metamorphism. Contributions to Mineralogy and Petrology 88, 246–259.

Wibberley, C., 1999. Are feldspar-to-mica reactions necessarily reaction-softening processes in fault zones. Journal of Structural Geology 21, 1219–1227.

Wibberley, C., 2005. Initiation of basement thrust detachments by fault-zone weakening. In: Bruhn, D., Burlini, L. (Eds.), High Strain Zones, Structure and Physical Properties. Geological Society, London, Special Publications, vol. 245, pp. 347–372.

Wintsch, R.P., Christoffersen, R., Kronenberg, A.K., 1995. Fluid–rock reaction weakening of fault zones. Journal of Geophysical Research 100, 13,021–13,032.

Wood, B.J., Walther, J.V., 1983. Rates of hydrothermal reactions. Science 222, 413–415.

Woodward, N.B., Gray, D.R., 1985. In: Woodward, N.B. (Ed.), Valley and Ridge Thrust Belt: Balanced Structural Sections, Pennsylvania to Alabama. Studies in Geology, vol. 12. Appalachian Basin Industrial Associates, University of Tennessee, p. 40.